THE JOURNAL OF PHYSICAL CHEMISTRY C
A JOURNAL OF THE AMERICAN CHEMICAL SOCIETY

pubs.acs.org/JPCC Article

# Black Phosphorus n-Type Doping by Cu: A Microscopic Surface Investigation

Abhishek Kumar, Francesca Telesio, Deborah Prezzi,* Claudia Cardoso, Alessandra Catellani, Stiven Forti, Camilla Coletti, Manuel Serrano−Ruiz, Maurizio Peruzzini, Fabio Beltram, and Stefan Heun*

Cite This: https://doi.org/10.1021/acs.jpcc.1c03531 Read Online

ACCESS | Metrics & More | Article Recommendations | Supporting Information

**ABSTRACT:** We study surface charge transfer doping of exfoliated black phosphorus (bP) flakes by copper using scanning tunneling microscopy (STM) and spectroscopy (STS) at room temperature. The tunneling spectra reveal a gap in correspondence of Cu islands, which is tentatively attributed to Coulomb blockade phenomena. Moreover, using line spectroscopic measurements across small copper islands, we exploit the potential of the local investigation, showing that the n-type doping effect of copper on bP is short-ranged. These experimental results are substantiated by first-principles simulations, which quantify the role of cluster size for an effective n-type doping of bP and show an electronic decoupling of the topmost bP layer from the underlying layers driven by the copper cluster, consistent with the Coulomb blockade interpretation. Our results provide novel understanding—difficult to retrieve by transport measurements—of the doping of bP by copper, which appears promising for the implementation of ultrasharp p−n junctions in bP.

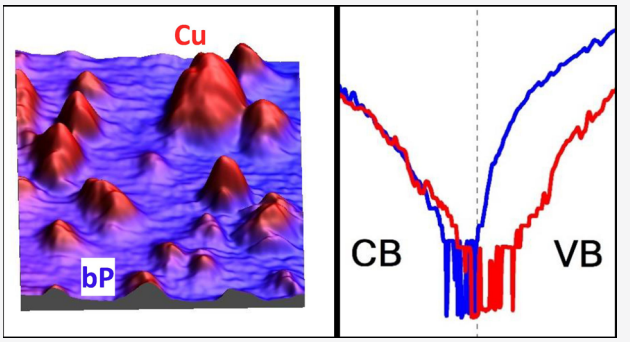


## INTRODUCTION

Black phosphorus (bP) is a semiconductor with a direct band gap that ranges from ∼0.3 (bulk) to ∼2.0 eV (monolayer) depending on layer thickness.[1−3] Among the van der Waals elemental materials,[4,5] bP in its few-layer form attracted great interest since its first exfoliation[6,7] because of the modulation of the direct band gap,[4,8] the in-plane anisotropy,[9−11] and its high charge-carrier mobility, up to 5200 $cm^2/(V\ s)$ at room temperature,[12] appealing for possible device applications.[13]

The presence of phosphorus vacancies, as reported in a recent scanning tunneling microscopy (STM) study,[14] makes bP an intrinsically p-doped material.[15,16] N-type doping of bP has been investigated in light of possible applications.[17] Several strategies have been pursued, from the reversible doping by field effect in transistors, where an ambipolar behavior was obtained,[1,18,19] to exfoliation of bulk crystals obtained by substitutional doping with Se[20] or Te.[21] A more promising strategy for few-layer flakes could be surface charge transfer doping, which has been implemented on several two-dimensional materials such as graphene[22,23] and transition metal dichalcogenides.[24,25] For bP, few studies report n-type doping by surface charge transfer,[26−34] mostly for the case of alkali metals.[27,31,32] Electrical transport measurements show n-type behavior when bP is doped by the deposition of copper.[28,33] However, no local spectroscopic investigation has been performed so far to understand the effect of Cu on the electronic properties of bP at the atomic level.

In this work, we performed an investigation of surface charge transfer doping by copper deposition on exfoliated bP flakes, combining STM and scanning tunneling spectroscopy (STS) measurements with first-principles calculations based on density functional theory (DFT). STS shows a gap in the spectra measured on Cu islands that we attribute to Coulomb blockade. The data also suggest that Cu induces an n-type doping in bP. Line-spectroscopic measurements across copper islands further show that the copper doping effect on bP is very short-ranged. Theoretical simulations reveal that Cu clusters efficiently decouple the topmost bP layer via charge localization, which explains both the Coulomb blockade as well as the local doping effect observed in experiments.

## RESULTS AND DISCUSSION

Figure 1 reports an STM analysis of copper deposited on bP flakes supported by a graphene-on-SiC substrate, which acts as

Received: April 20, 2021
Revised: May 31, 2021

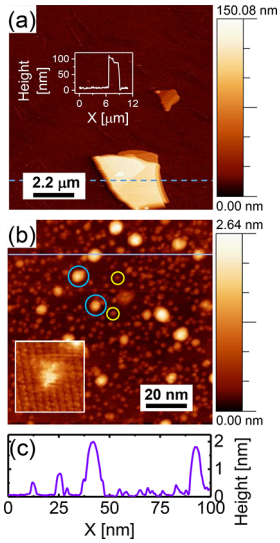


**Figure 1.** (a) 11 $\mu$m × 11 $\mu$m STM image showing two bP flakes on a graphene substrate after 20 min of copper deposition. Scan parameters: (− 3.0 V, 0.33 nA). Inset: height profile across the larger flake along the dashed blue line. The flake has two plateaus; the higher region (top part of the flake) is 93 nm high, the lower (bottom part) 80 nm. All measurements presented in the following panels were performed on the lower plateau. (b) 100 nm × 100 nm STM image on the larger flake, showing copper islands on bP. Some of the smaller and larger copper islands are identified by yellow and blue circles, respectively. Inset: 5 nm × 5 nm STM image obtained upon further zoom-in, showing a copper island on top of the atomically resolved bP surface. Scan parameters for both images: (− 1.0 V, 0.33 nA). (c) Height profile along the violet line in panel b.

a conductive ground electrode.[35] A comparison of bP surfaces before and after copper deposition is shown in the Supporting Information (Figure S2), where the pristine bP surface appears clean and flat at this magnification, with some defects related to intrinsic phosphorus vacancies, consistent with previous reports.[14,35,36] Figure 1a shows two representative bP flakes on which copper was deposited for 20 min. A zoom-in on the larger flake (Figure 1b) shows bright features on the surface that appear only after copper deposition and are therefore identified as copper islands, indicative of a Volmer−Weber growth mode. Copper islands of two different sizes can be seen, indicated by blue (larger islands, diameter 7.84 ± 1.08 nm, height 1.91 ± 0.31 nm) and yellow circles (smaller islands, diameter 3.75 ± 0.51 nm, height 0.63 ± 0.11 nm). From a statistical analysis of several different spots on the flake, we compute a coverage of 0.80 ± 0.11 ML of copper on the bP surface.[37] We underline that these islands are rather different from the chiral Cu structures that were recently reported and were obtained upon heating of Cu nanoparticles on bP flakes at 300 °C.[38]

A further zoom-in on the flake is shown in the inset of Figure 1b. The surface shows the zigzag pattern characteristic of the [100] direction of bP[35] and a copper island on top of it. This observation allows us to exclude an intercalation of the Cu here since in that case the typical lattice structure of bP should be visible also on top of the intercalated copper, as observed in similar systems such as lithium-intercalated graphene.[39] The fact that the edges of the copper island appear fuzzy when imaged at high resolution is a sign of thermally activated motion of copper atoms at room temperature.[40] Despite this motion, however, the copper islands are stable, since their relative positions remain unchanged in multiple scans of the same location (Figure S3). This excludes any tip-induced effects and is in contrast to other reports, where motion or modification of islands on the substrate was induced by the tip of an STM.[41,42]

This structural microscopic investigation by STM is coupled to DFT-based ab initio simulations addressing the formation energies of the main Cu point defects and adatoms on few-layer bP slabs, together with adsorbed clusters of increasing size. Figure 2a illustrates the single Cu impurities investigated here: substitutional ($Cu_s$), interstitial ($Cu_i$), and adsorbed copper in four different adsorption sites, i.e., hollow ($Cu_H$), top ($Cu_T$), and two bridge sites ($Cu_{B_1}$ and $Cu_{B_2}$, bridging atoms on adjacent zigzag rows and adjacent atoms on the same zigzag row, respectively). According to the values reported in Table 1, $Cu_s$ saturating P vacancies is the most stable point defect,

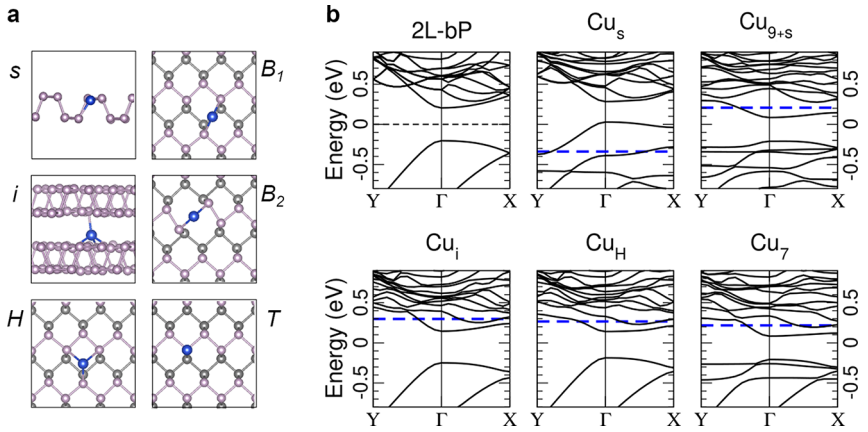


**Figure 2.** (a) Ball-and-stick models for single Cu impurities (blue spheres) in bP. The interstitial, i, and substitutional, s, sites are shown as side views. For adsorbed Cu atoms, several sites were considered, that is hollow (H), top (T) and two different bridge positions ($B_1$ and $B_2$), shown as top views. For the top views, the bottom phosphorus layer is represented in gray, in order to make the figures clearer. (b) Band structure of the three lowest energy Cu impurities and two representative Cu clusters. The band structure of pristine 2L-bP is reported for comparison, the midgap of which is set as the zero energy reference for all band structures. The Fermi level of the different Cu configurations is highlighted by dashed blue lines. The high-symmetry points X and Y indicate the zone-center along the zigzag and armchair direction, respectively.


https://doi.org/10.1021/acs.jpcc.1c03531
J. Phys. Chem. C XXXX, XXX, XXX−XXX

followed by $Cu_i$, while single Cu adatoms are preferentially adsorbed in a hollow position ($Cu_H$).

**Table 1. Formation Energy ($\Delta E$) of Cu Single Impurities (Left) and Cu Clusters (Right) on bP at $T$ = 0 K[a]**

| site | $\Delta E$ (eV) | cluster | $\Delta E/N_{Cu}$ (eV) | $\delta E/N_{Cu_{ads}}$ (eV) |
|---|---|---|---|---|
| s | −4.47 | $Cu_{1+s}$ | −4.01 | −0.87 |
| i | −3.46 | $Cu_{3+s}$ | −3.56 | −0.58 |
| H | −2.68 | $Cu_{7+s}$ | −3.36 | −0.51 |
| $B_1$ | −2.55 | $Cu_{9+s}$ | −3.42 | −0.62 |
| $B_2$ | −1.61 | $Cu_3$ | −2.85 | −0.08 |
| T | −1.51 | $Cu_7$ | −3.03 | −0.35 |

[a]For Cu adatoms, several sites were considered, that is hollow (H), top (T), and two different bridge positions ($B_1$ and $B_2$). The formation energy of adsorbed Cu clusters of increasing size is reported per Cu atom, while the energy gain with respect to the single impurities is per Cu adsorbed atom. Clusters are labeled as $Cu_{n+s}$ ($n$ Cu atoms added to the $Cu_s$ impurity) and $Cu_n$ ($n$ adsorbed Cu atoms including the initial $Cu_H$).

The formation of clusters on the bP surface is also investigated, as shown in Table 1, starting from the most stable single Cu impurities decorating the surface, i.e., $Cu_s$ and $Cu_H$. In particular, we considered two series of clusters as obtained by using either a surface substitutional $Cu_s$ or a single adsorbed $Cu_H$ atom as nucleus and adding further Cu atoms to build clusters of increasing size. The two series are hereafter labeled as $Cu_{n+s}$ ($n$ Cu atoms added to the $Cu_s$ impurity) and $Cu_n$ ($n$ adsorbed Cu atoms including the initial $Cu_H$). In addition to the formation energy per Cu atom, Table 1 reports also the energy gain for the clusters with respect to the isolated impurities per adsorbed Cu atom (last column): this value indicates that cluster formation is always favored, in overall agreement with experimental observations, which do not evidence single Cu atoms on the surface at room temperature. More specifically, we find that cluster nucleation around $Cu_s$ sites is the (thermodynamically) most favorable process.

For a better understanding of the electronic properties of Cu on bP, we report in Figure 2b the computed DFT band structure for the three lowest-energy isolated Cu impurities discussed above, i.e., $Cu_s$, $Cu_i$, and $Cu_H$, together with the band structure of selected adsorbed clusters. The band structure of pristine 2-layer (2L-) bP is shown as a reference. Starting with the single Cu impurities, we notice that $Cu_i$ and $Cu_H$ behave as n-type dopants whereas substitutional copper leads to a p-doping of bP. While for the n-doped systems ($Cu_i$ and $Cu_H$) the valence band is very similar to the pristine one, the p-doped system ($Cu_s$) has a markedly different valence-band structure. In all cases, the band gap is either reduced (by up to 150 meV for $Cu_s$) or almost unchanged ($Cu_i$)[43] in the presence of Cu atoms, as previously observed for other TM adatoms.[44,45]

Considering now the clusters, the doping effect for $Cu_7$, which is adsorbed on the pristine surface, is very similar to that of a single Cu adatom ($Cu_H$), i.e., n-type, and shows only some additional nondispersive Cu states in the region close to the band gap. In the case of clusters building on a substitutional $Cu_s$ seed ($Cu_{n+s}$), the n-type doping effect of the cluster tends to overcome the p-type doping character of the $Cu_s$ seed for sufficiently large clusters, resulting in a band structure similar to that of the adsorbed clusters without seed, as can be seen by comparing $Cu_{9+s}$ and $Cu_7$. This points to the existence of a critical size at which all Cu clusters would behave the same, i.e., n-doping and band gap reduction, irrespective of the presence of a substitutional seed.

We further investigate the band gap modification and doping induced by copper clusters by focusing on $Cu_7$ and consider a larger supercell (5 × 5) and a thicker bP slab (3-layer, 3L) to minimize the effect due to periodic replicas. The results are shown in Figure 3. A similar analysis for the case of $Cu_{7+s}$ is reported in the Supporting Information (Figure S4). Figure 3a shows the projected density of states (pDOS) of $Cu_7$ on 3L-bP separated into the contribution of Cu atomic orbitals (orange curve) and the atomic orbitals of each bP layer (violet and light blue). Panel b shows the band structure computed for the

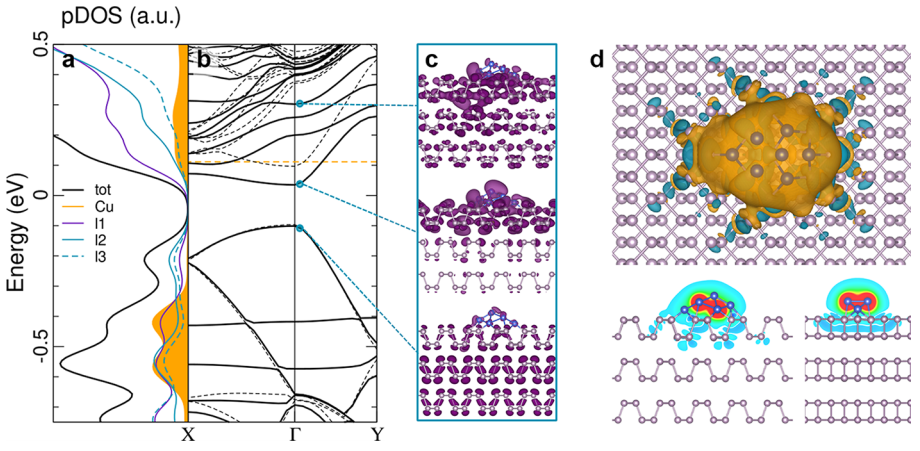


**Figure 3.** Electronic properties of adsorbed $Cu_7$ on 3L-bP. (a) The total density of states (black line) is split into the contribution of the Cu cluster (orange curve) and bP first (l1), second (l2), and third layers (l3) by using atomic projections. (b) The band structure in the presence of the adsorbed Cu cluster (solid black line) is compared to that of pristine 3L-bP (dashed line). The Fermi level of the doped system is also reported (orange dashed line), with the midgap of the pristine 3L-bP set as the zero energy reference. (c) A few relevant Kohn−Sham squared wave functions are displayed, with purple (blue) balls denoting P (Cu) atoms. The isosurface amplitude is $7 \times 10^{-5}$ a.u. (d) Top-view of the charge density difference with an isosurface amplitude of $3 \times 10^{-4}$ a.u. (top panel, orange (blue) is the positive (negative) isosurface), together with two sections of the isosurface along armchair and zigzag directions (bottom panel). For the sections, we use a RGB color scale with red and blue corresponding to +0.03 and −0.008, respectively.


https://doi.org/10.1021/acs.jpcc.1c03531
J. Phys. Chem. C XXXX, XXX, XXX−XXX

$Cu_7$/3L-bP case, as compared to the band structure of pristine 3L-bP (black dashed lines). While the band structure highlights the same qualitative features described above for $Cu_7$/2L-bP (see Figure 2), the pDOS shows that the copper affects mainly the topmost bP layer, which presents Cu-derived peaks at about −0.4 and +0.15 eV (l1, violet line). At these energies, the contributions from the bottom bP layers (l2 and l3, light blue) are instead significantly smaller. This suggests that the Cu levels around the band gap region hybridize mainly with states localized in the topmost bP layer and are essentially decoupled from the layers underneath. In contrast, deeper Cu-originating states hybridize with states from all three bP layers.

This is confirmed by the plot of the Kohn−Sham orbitals for selected states (Figure 3c). Indeed, the orbitals at the bottom of the conduction band are spatially localized at the topmost bP layer. Only at higher energies, the wave functions are distributed over the entire system (i.e., similar to those of pristine bP). Deeper insight into the charge-density redistribution upon Cu doping can be obtained by plotting the charge-density difference for the $Cu_7$/3L-bP system, obtained by subtracting the charge computed for the pristine substrate from the total charge of the doped system (see Figure 3d). From both the top view of the isosurface plot (top panel) and the isosurface sections along the zigzag and armchair directions (bottom panels), we note that (i) the Cu charge transferred to bP remains mostly localized on the topmost layer and (ii) the charge shows a strong localization in the bP plane around the cluster, with an abrupt decay within a few lattice units. In addition, the charge rearrangement in the stacking direction reveals the origin of the spatial localization of the frontier orbitals described above as a result of the local field generated at the interface, reminiscent of what is found in the presence of an applied external electric field.[46,47] This finds a correspondence in the potential energy difference (or workfunction difference) between the top (i.e., doped side) and bottom of the Cu-decorated bP slab, which is positive for the n-type doped $Cu_7$/3L-bP system and amounts to 98 meV.

Taking advantage of the DFT analysis, we next move to local spectroscopy by STS, both on flat bP surface areas and on copper islands. Typical differential-conductance curves are shown in Figure 4, where both linear and logarithmic plots are displayed for an analysis of spectral shape and identification of the gap region, respectively. The shape of the spectra recorded off the copper islands (Figure 4a), with a larger amplitude at positive tip bias, very much resembles that of pristine bP.[14,48] On the contrary, the spectra measured on copper islands (Figure 4c) display similar spectral amplitude at ±1 V and thus a more symmetric shape. We can exclude that the shape of the spectra is affected by thermal drift of the STM tip in $z$-direction, since we have checked that for all spectra the forward and backward sweeps were coinciding (as shown in the Supporting Information).

From more than 40 spectra measured in several spots on the flake, we obtain a gap value of 0.25 ± 0.10 eV for the flat bP areas, consistent with the reported band gap value of pristine bP.[14,15,36,48] As shown in Figure 4b, the position of the Fermi level (at zero bias, vertical black dot-dash line) is lying close to the valence-band edge, which implies p-type doping, consistent with the literature for pristine bP.[14] Thus, the spectra measured on the flat bP surface away from Cu islands can be attributed to pristine bP. The same analysis for spectra recorded on copper islands gives a gap value of 0.46 ± 0.20 eV.

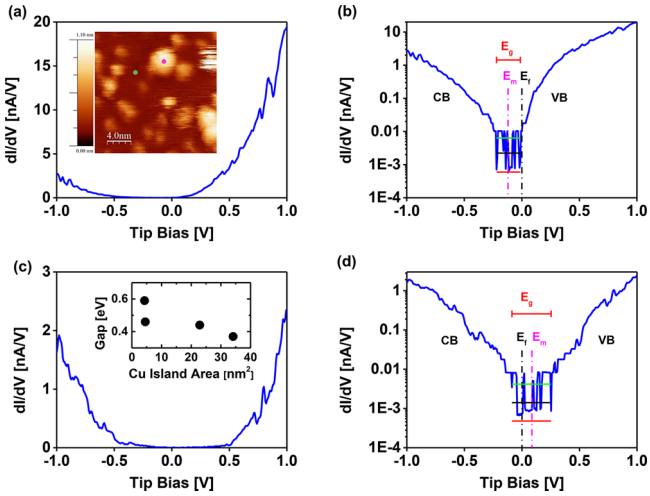


**Figure 4.** Differential conductance ($dI/dV$) spectra (a) for pristine bP and (c) for Cu on bP. The green and the pink spots in the STM image shown as an inset to panel a indicate where the spectra in panels a and c, respectively, were recorded. The same spectra as in panels a and c are plotted on a logarithmic scale in panels b and d for pristine bP and Cu on bP, respectively. The inset to panel c shows how the gap measured on Cu islands changes with island area. Scan parameters of the STM image in panel a and STS set point for all spectra (on bP and Cu islands): (−1.0 V, 0.33 nA). The bias is applied to the tip.

To determine the gap values, we followed the procedure described in ref 14.

Even though the increase in the band gap and the symmetry of the differential-conductance curves in the presence of the Cu islands are in apparent contradiction with the DFT results described above, the results can be consistently understood if we invoke a Coulomb blockade for the Cu islands. Similar effects have already been observed in the single-electron tunneling spectra of ultrasmall metal islands at room temperature.[49−51] Here, DFT calculations show that close to the Fermi level, the localized frontier states do not hybridize with the lower bP layers, thus creating a tunnel barrier between the Cu islands and the bP bulk. In this situation, the electron charge on the Cu islands can be quantized if two conditions are met:[49,52] (i) The capacitance $C$ of the islands is sufficiently small such that the charging energy $e^2/2C$ exceeds the thermal energy $k_BT$. Here, applying a parallel plate capacitor model,[53] we estimate $C \approx 10^{-18}$ F, which leads to $e^2/2C \approx 100$ meV, larger than $k_BT$ (~25 meV at room temperature). (ii) The tunneling resistance $R_T$ between STM tip and Cu island is much larger than the resistance quantum $R_K = h/e^2 \approx 25.8$ kΩ. From Figure 4d, we get $R_T > 10$ GΩ for $V_{tip} < \pm 0.5$ V. Being in a situation in which these two conditions are met, it is reasonable to conclude that the experimentally observed gap might be due to Coulomb blockade. Consistently, a Coulomb gap of 0.45 eV ($= e/C$)[53] corresponds to a capacitance $C = 4 \times 10^{-19}$ F, in good agreement with the estimate based on the parallel plate capacitor model. A further evidence of Coulomb blockade effect is given by the gap dependence with the island dimension. As shown in the inset to Figure 4c, the experimentally observed gap decreases with increasing island area, as expected for Coulomb blockade,[54] approaching the value of the bP band gap for the largest island measured.

The STS data in Figure 4d, which was measured on a Cu island, shows that the position of the Fermi level does not


https://doi.org/10.1021/acs.jpcc.1c03531
J. Phys. Chem. C XXXX, XXX, XXX−XXX

coincide with the midgap position but is shifted toward the conduction band edge. According to the orthodox theory of tunneling through a double junction, which applies here,[54] the asymmetric gap observed in Figure 4d is due to the fractional residual charge $Q_0$ on the Cu island.[55] According to Hanna and Tinkham,[55] $Q_0$ originates from the difference in work function, or the contact potential, across the junctions. $Q_0$ is then obtained from

$$Q_0 = \frac{1}{e}[C_1\Delta\Phi_1 - C_2\Delta\Phi_2] \quad (1)$$

with $C_i$ the capacitance of junction $i$ and $\Delta\Phi_i$ the difference in work function across junction $i$; $i = 1$ indicates the tip-island junction and $i = 2$ the island-substrate junction. Here, we observe a positive $Q_0 > 0$, and thus a positive value of the contact potential, which indicates an n-type doping of the bP, in agreement with our DFT calculations and literature.[28,33]

To corroborate these results and determine experimentally the length scale of the electronic effect driven by copper, we performed line-spectroscopic measurements across copper islands, as shown in Figure 5. We measured in total five different copper islands, and we see line spectra showing consistent behavior. Figure 5 shows a series of tunneling spectra laterally separated from each other by ∼2 nm. The measurement spots follow a path across a copper island, as shown in Figure 5b. The individual spots are color-coded, from blue, the starting point of the path, to pink, the end point of the path, both of which lie on the flat bP surface. The copper island lies in between, with the corresponding green spots. For each spot, six spectra were recorded, and the resulting averages are shown in Figure 5a, using the same colors. The blue and pink curves, corresponding to the data from bP, are clearly different from the green curves measured on the copper island. These observations are consistent with the spectra shown in Figure 4 and thus demonstrate how reproducible these spectral features are, and indicate a negligible drift of the tip during the line STS measurement.

A height profile across the Cu island is reported in Figure 5c, with two vertical dashed red lines marking the extremes of the island. Figures 5b–d have the same $x$-axis, corresponding to the scan size of the STM image. The midgap values obtained from the spectra shown in Figure 5a are plotted versus lateral position in Figure 5d. A clear transition from p-type (n-type) to n-type (p-type) behavior can be seen in correspondence of the extremes of the Cu island. The data points of Figure 5d are well fitted with a Gaussian curve, centered at 10.78 ± 0.17 nm with a fwhm of 3.96 ± 0.47 nm, in excellent agreement with the center of the copper island. Our experimental observations are in good agreement with the results shown in Figure 3d and consistent with a strong quantum confinement of charge transfer from copper to bP. Using the same technique of line-spectroscopic measurements, similar short-ranged spectral features have been previously reported for N-doped graphene[56] and P-vacancies in bP.[14]

Our local investigation of bP doping induced by copper islands shows that only the regions of bP lying in close proximity to copper islands are significantly n-type doped, while the regions of bP few nanometers away from the copper islands still retain their intrinsic p-type doping. Thus, the presence of isolated Cu-islands on bP implies the formation of localized n-doped regions surrounded by intrinsic bP p-doped regions. We anticipate that decreasing the copper island size and increasing their density will result in homogeneously

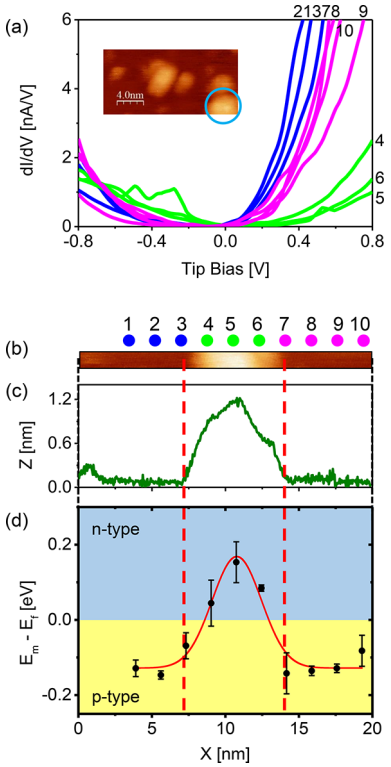


**Figure 5.** Line STS across a single copper island. (a) Average spectra recorded along a line across a copper island, numbered corresponding to lateral spots shown in panels b. The copper island is shown in the 20 nm × 10 nm STM image in the inset (indicated by the blue circle). (b) 20 nm × 1 nm STM image of the copper island on bP on which the line STS measurement was performed. Spots of individual measurements are indicated by blue, green, and pink dots. (c) Height profile across the island. (d) Midgap value of individual spectra with respect to the Fermi level, plotted as a function of lateral position. The plot field is colored with yellow and blue to indicate p-type and n-type doping regions, respectively. The $x$-axes in panels b–d are the same. Two vertical dashed red lines show the position of the edges of the copper island. Scan parameters of the STM images in panels a and b and STS set point for all spectra: (−1.0 V, 0.33 nA). Between the spectra taken at various points along the line, the feedback loop was engaged.

doped n-type bP samples. Technically, this could be achieved by sputter-deposition of Cu, as already demonstrated by Koenig et al.[28] An alternative approach could be based on our result that Cu clusters preferentially nucleate at $Cu_s$ sites. Thus, one might influence the distribution of Cu by a defect engineering of the P vacancies, for example by an ion bombardment of the bP surface prior to Cu deposition.

In summary, our study provides a combined experimental and theoretical in-depth understanding of the doping behavior of Cu on bP at the nanoscale. STS measurements suggest Coulomb blockade in the Cu islands and an n-type doping in bP after Cu deposition, consistent with DFT predictions. The DFT analysis also shows a decoupling of the topmost bP layer in the presence of copper. Line-spectroscopy measurements finally highlight that the doping effect of Cu on bP is short ranged, in good agreement with the results of our DFT calculations. This first STM investigation of Cu-doped bP at the nanoscale is of significant importance both for a fundamental understanding of the doping mechanisms and in view of potential applications of this material in electronics. Our results indicate a route toward ultrasharp p–n junctions in


https://doi.org/10.1021/acs.jpcc.1c03531
J. Phys. Chem. C XXXX, XXX, XXX−XXX

bP, which would be exciting to explore in transport measurements on high-mobility bP and might enable observation of electro-optical effects in this material.[57]

## METHODS

Thin flakes of bP were prepared using the scotch tape exfoliation method. The exfoliated bP flakes were transferred onto monolayer graphene grown epitaxially on silicon carbide. This graphene film was used as a substrate and connected to ground potential. Details of sample preparation are reported elsewhere.[35] Typical dimensions of the bP flakes are area 2.7 ± 3.2 $\mu m^2$ and thickness 37.5 ± 22.4 nm. All measurements presented here were performed on a flake 80 nm-thick. Copper was then deposited in situ via thermal evaporation using an EFM-3S e-beam evaporator, and surface investigations were performed at room temperature using an Omicron LT-STM. Theoretical investigation of both stability and electronic properties of Cu-doped bP was carried out by using a first-principles plane-wave pseudopotential implementation of density functional theory (DFT), as available in the Quantum ESPRESSO package.[58,59] The Perdew–Burke–Ernzerhof (PBE) generalized gradient approximation for the exchange-correlation functional was used,[60] and dispersion corrections were included within the semiempirical method developed by Grimme (DFT-D2).[61] Ultrasoft pseudopotentials were employed as available in the SSSP Library.[62] Further details on experiment and theory are reported in the Supporting Information.

## ASSOCIATED CONTENT

### Supporting Information

The Supporting Information is available free of charge at https://pubs.acs.org/doi/10.1021/acs.jpcc.1c03531.

Extended experimental methods, Raman spectroscopy measurements, STM images of bP surfaces before and after Cu deposition, stability of Cu islands, numerical details of DFT simulations, and complementary data (PDF)

## AUTHOR INFORMATION


### Corresponding Authors

**Deborah Prezzi** − *S3, Istituto Nanoscienze-CNR, 41125 Modena, Italy*; orcid.org/0000-0002-7294-7450; Email: deborah.prezzi@nano.cnr.it

**Stefan Heun** − *NEST, Istituto Nanoscienze−CNR and Scuola Normale Superiore, 56127 Pisa, Italy*; orcid.org/0000-0003-1989-5679; Email: stefan.heun@nano.cnr.it

### Authors

**Abhishek Kumar** − *NEST, Istituto Nanoscienze−CNR and Scuola Normale Superiore, 56127 Pisa, Italy*; orcid.org/0000-0001-7676-7927

**Francesca Telesio** − *NEST, Istituto Nanoscienze−CNR and Scuola Normale Superiore, 56127 Pisa, Italy*; orcid.org/0000-0003-3834-3685

**Claudia Cardoso** − *S3, Istituto Nanoscienze-CNR, 41125 Modena, Italy*

**Alessandra Catellani** − *S3, Istituto Nanoscienze-CNR, 41125 Modena, Italy*; orcid.org/0000-0001-5197-7186

**Stiven Forti** − *Center for Nanotechnology Innovation @ NEST, Istituto Italiano di Tecnologia, 56127 Pisa, Italy*

**Camilla Coletti** − *Center for Nanotechnology Innovation @ NEST, Istituto Italiano di Tecnologia, 56127 Pisa, Italy*; orcid.org/0000-0002-8134-7633

**Manuel Serrano−Ruiz** − *CNR-ICCOM, 50019 Sesto Fiorentino, Italy*

**Maurizio Peruzzini** − *CNR-ICCOM, 50019 Sesto Fiorentino, Italy*; orcid.org/0000-0002-2708-3964

**Fabio Beltram** − *NEST, Istituto Nanoscienze−CNR and Scuola Normale Superiore, 56127 Pisa, Italy*

Complete contact information is available at: https://pubs.acs.org/10.1021/acs.jpcc.1c03531


### Notes

The authors declare no competing financial interest.

## ACKNOWLEDGMENTS

Useful discussions with Thomas Szkopek and Hervé Courtois are gratefully acknowledged. F.T. and D.P. acknowledge financial support by CNR-Nano through the SEED project SURPHOS. We thank the European Research Council for funding the project PHOSFUN *Phosphorene functionalization: a new platform for advanced multifunctional materials* (Grant Agreement No. 670173) through an ERC Advanced Grant to MP. Computational resources were partly granted by the Center for Functional Nanomaterials at Brookhaven National Laboratory, supported by the U.S. Department of Energy, Office of Basic Energy Sciences, under Contract No. DE-SC0012704.

## REFERENCES


(1) Das, S.; Zhang, W.; Demarteau, M.; Hoffmann, A.; Dubey, M.; Roelofs, A. Tunable Transport Gap in Phosphorene. *Nano Lett.* **2014**, *14*, 5733−5739.

(2) Tran, V.; Soklaski, R.; Liang, Y.; Yang, L. Layer-controlled band gap and anisotropic excitons in few-layer black phosphorus. *Phys. Rev. B: Condens. Matter Mater. Phys.* **2014**, *89*, 235319.

(3) Roldán, R.; Castellanos-Gomez, A. Black phosphorus: A new bandgap tuning knob. *Nat. Photonics* **2017**, *11*, 407−409.

(4) Ling, X.; Wang, H.; Huang, S.; Xia, F.; Dresselhaus, M. S. The renaissance of black phosphorus. *Proc. Natl. Acad. Sci. U. S. A.* **2015**, *112*, 4523−4530.

(5) Peruzzini, M.; Bini, R.; Bolognesi, M.; Caporali, M.; Ceppatelli, M.; Cicogna, F.; Coiai, S.; Heun, S.; Ienco, A.; Benito, I. I.; Kumar, A.; Manca, G.; Passaglia, E.; Scelta, D.; Serrano-Ruiz, M.; Telesio, F.; Toffanin, S.; Vanni, M.; et al. A Perspective on Recent Advances in Phosphorene Functionalization and Its Applications in Devices. *Eur. J. Inorg. Chem.* **2019**, *2019*, 1476−1494.

(6) Castellanos-Gomez, A.; Vicarelli, L.; Prada, E.; Island, J. O.; Narasimha-Acharya, K. L.; Blanter, S. I.; Groenendijk, D. J.; Buscema, M.; Steele, G. A.; Alvarez, J. V.; et al. Isolation and characterization of few-layer black phosphorus. *2D Mater.* **2014**, *1*, 025001.

(7) Liu, H.; Neal, A. T.; Zhu, Z.; Luo, Z.; Xu, X.; Tománek, D.; Ye, P. D. Phosphorene: An Unexplored 2D Semiconductor with a High Hole Mobility. *ACS Nano* **2014**, *8*, 4033−4041.

(8) Churchill, H. O. H.; Jarillo-Herrero, P. Phosphorus joins the family. *Nat. Nanotechnol.* **2014**, *9*, 330.

(9) Xia, F.; Wang, H.; Jia, Y. Rediscovering black phosphorus as an anisotropic layered material for optoelectronics and electronics. *Nat. Commun.* **2014**, *5*, 4458.

(10) Lee, S.; Yang, F.; Suh, J.; Yang, S.; Lee, Y.; Li, G.; Sung Choe, H.; Suslu, A.; Chen, Y.; Ko, C.; et al. Anisotropic in-plane thermal conductivity of black phosphorus nanoribbons at temperatures higher than 100 K. *Nat. Commun.* **2015**, *6*, 8573.

(11) Telesio, F.; Hemsworth, N.; Dickerson, W.; Petrescu, M.; Tayari, V.; Yu, O.; Graf, D.; Serrano-Ruiz, M.; Caporali, M.; Peruzzini,

M.; et al. Nonclassical Longitudinal Magnetoresistance in Anisotropic Black Phosphorus. *Phys. Status Solidi RRL* **2020**, *14*, 1900347.
(12) Long, G.; Maryenko, D.; Shen, J.; Xu, S.; Hou, J.; Wu, Z.; Wong, W. K.; Han, T.; Lin, J.; Cai, Y.; et al. Achieving Ultrahigh Carrier Mobility in Two-Dimensional Hole Gas of Black Phosphorus. *Nano Lett.* **2016**, *16*, 7768−7773.
(13) Huang, H.; Jiang, B.; Zou, X.; Zhao, X.; Liao, L. Black phosphorus electronics. *Science Bulletin* **2019**, *64*, 1067−1079.
(14) Kiraly, B.; Hauptmann, N.; Rudenko, A. N.; Katsnelson, M. I.; Khajetoorians, A. A. Probing Single Vacancies in Black Phosphorus at the Atomic Level. *Nano Lett.* **2017**, *17*, 3607−3612.
(15) Morita, A. Semiconducting black phosphorus. *Appl. Phys. A: Solids Surf.* **1986**, *39*, 227−242.
(16) Narita, S.; Akahama, Y.; Tsukiyama, Y.; Muro, K.; Mori, S.; Endo, S.; Taniguchi, M.; Seki, M.; Suga, S.; Mikuni, A.; Kanzaki, H.; et al. Electrical and optical properties of black phosphorus single crystal. *Physica B+C* **1983**, *117−118*, 422−424.
(17) Hu, H.; Shi, Z.; Khan, K.; Cao, R.; Liang, W.; Tareen, A. K.; Zhang, Y.; Huang, W.; Guo, Z.; Luo, X.; et al. Recent advances in doping engineering of black phosphorus. *J. Mater. Chem. A* **2020**, *8*, 5421−5441.
(18) Perello, D. J.; Chae, S. H.; Song, S.; Lee, Y. H. High-performance n-type black phosphorus transistors with type control via thickness and contact-metal engineering. *Nat. Commun.* **2015**, *6*, 7809.
(19) Xu, Y.; Yuan, J.; Zhang, K.; Hou, Y.; Sun, Q.; Yao, Y.; Li, S.; Bao, Q.; Zhang, H.; Zhang, Y. Field-Induced n-Doping of Black Phosphorus for CMOS Compatible 2D Logic Electronics with High Electron Mobility. *Adv. Funct. Mater.* **2017**, *27*, 1702211.
(20) Xu, Y.; Yuan, J.; Fei, L.; Wang, X.; Bao, Q.; Wang, Y.; Zhang, K.; Zhang, Y. Selenium-Doped Black Phosphorus for High-Responsivity 2D Photodetectors. *Small* **2016**, *12*, 5000−5007.
(21) Yang, B.; Wan, B.; Zhou, Q.; Wang, Y.; Hu, W.; Lv, W.; Chen, Q.; Zeng, Z.; Wen, F.; Xiang, J.; et al. Te-Doped Black Phosphorus Field-Effect Transistors. *Adv. Mater.* **2016**, *28*, 9408−9415.
(22) Chen, W.; Chen, S.; Qi, D. C.; Gao, X. Y.; Wee, A. T. S. Surface transfer p-type doping of epitaxial graphene. *J. Am. Chem. Soc.* **2007**, *129*, 10418−10422.
(23) Starke, U.; Forti, S.; Emtsev, K. V.; Coletti, C. Engineering the electronic structure of epitaxial graphene by transfer doping and atomic intercalation. *MRS Bull.* **2012**, *37*, 1177−1186.
(24) Zhang, S.; Hill, H. M.; Moudgil, K.; Richter, C. A.; Hight Walker, A. R.; Barlow, S.; Marder, S. R.; Hacker, C. A.; Pookpanratana, S. J. Controllable, Wide-Ranging n-Doping and p-Doping of Monolayer Group 6 Transition-Metal Disulfides and Diselenides. *Adv. Mater.* **2018**, *30*, 1802991.
(25) Xu, K.; Wang, Y.; Zhao, Y.; Chai, Y. Modulation doping of transition metal dichalcogenide/oxide heterostructures. *J. Mater. Chem. C* **2017**, *5*, 376−381.
(26) Xiang, D.; Han, C.; Wu, J.; Zhong, S.; Liu, Y.; Lin, J.; Zhang, X.-A.; Ping Hu, W.; Özyilmaz, B.; Neto, A. H. C.; et al. Surface transfer doping induced effective modulation on ambipolar characteristics of few-layer black phosphorus. *Nat. Commun.* **2015**, *6*, 6485.
(27) Kim, J.; Baik, S. S.; Ryu, S. H.; Sohn, Y.; Park, S.; Park, B.-G.; Denlinger, J.; Yi, Y.; Choi, H. J.; Kim, K. S. Observation of tunable band gap and anisotropic Dirac semimetal state in black phosphorus. *Science* **2015**, *349*, 723−726.
(28) Koenig, S. P.; Doganov, R. A.; Seixas, L.; Carvalho, A.; Tan, J. Y.; Watanabe, K.; Taniguchi, T.; Yakovlev, N.; Castro Neto, A. H.; Özyilmaz, B. Electron Doping of Ultrathin Black Phosphorus with Cu Adatoms. *Nano Lett.* **2016**, *16*, 2145−2151.
(29) Yu, X.; Zhang, S.; Zeng, H.; Wang, Q. J. Lateral black phosphorene P-N junctions formed via chemical doping for high performance near-infrared photodetector. *Nano Energy* **2016**, *25*, 34−41.
(30) Cho, S. Y.; Koh, H. J.; Yoo, H. W.; Jung, H. T. Tunable Chemical Sensing Performance of Black Phosphorus by Controlled Functionalization with Noble Metals. *Chem. Mater.* **2017**, *29*, 7197−7205.
(31) Gao, T.; Li, X.; Xiong, X.; Huang, M.; Li, T.; Wu, Y. Optimized Transport Properties in Lithium Doped Black Phosphorus Transistors. *IEEE Electron Device Lett.* **2018**, *39*, 769−772.
(32) Kiraly, B.; Knol, E. J.; Volckaert, K.; Biswas, D.; Rudenko, A. N.; Prishchenko, D. A.; Mazurenko, V. G.; Katsnelson, M. I.; Hofmann, P.; Wegner, D.; et al. Anisotropic two-dimensional screening at the surface of black phosphorus. *Phys. Rev. Lett.* **2019**, *123*, 216403.
(33) Lin, Z.; Wang, J.; Guo, X.; Chen, J.; Xu, C.; Liu, M.; Liu, B.; Zhu, Y.; Chai, Y. Interstitial copper-doped edge contact for n-type carrier transport in black phosphorus. *InfoMat* **2019**, *1*, 242−250.
(34) Ou, P.; Zhou, X.; Chen, C.; Meng, F.; Chen, Y.; Song, J. Reduction of Fermi level pinning at Cu-BP interfaces by atomic passivation. *Nanoscale* **2019**, *11*, 11569−11576.
(35) Kumar, A.; Telesio, F.; Forti, S.; Al-Temimy, A.; Coletti, C.; Serrano-Ruiz, M.; Caporali, M.; Peruzzini, M.; Beltram, F.; Heun, S. STM study of exfoliated few layer black phosphorus annealed in ultrahigh vacuum. *2D Mater.* **2019**, *6*, 015005.
(36) Riffle, J. V.; Flynn, C.; St Laurent, B.; Ayotte, C. A.; Caputo, C. A.; Hollen, S. M. Impact of vacancies on electronic properties of black phosphorus probed by STM. *J. Appl. Phys.* **2018**, *123*, 044301.
(37) To quantify copper coverage, we calculated the volume of copper islands in STM images by flooding analysis and normalized it by the amount of copper required for a uniform monolayer (ML) coverage. We define 1 ML as $1.767 \times 10^{15}$ atoms/cm$^2$. To get this number, we used 8.96 g/cm$^3$ as the copper density, $1.055 \times 10^{-22}$ g as copper atomic mass, and 2.08 Å as the spacing between (111) planes in the Cu fcc lattice.[63]
(38) Nerl, H. C.; Pokle, A.; Jones, L.; Muller-Caspary, K.; Bos, K. H. W.; Downing, C.; McCarthy, E. K.; Gauquelin, N.; Ramasse, Q. M.; Lobato, I.; Daly, D.; Idrobo, J. C.; Van Aert, S.; Van Tendeloo, G.; Sanvito, S.; Coleman, J. N.; Cucinotta, C. S.; Nicolosi, V.; et al. Self-Assembly of Atomically Thin Chiral Copper Heterostructures Templated by Black Phosphorus. *Adv. Funct. Mater.* **2019**, *29*, 1903120.
(39) Fiori, S.; Murata, Y.; Veronesi, S.; Rossi, A.; Coletti, C.; Heun, S. Li-intercalated graphene on SiC(0001): An STM study. *Phys. Rev. B: Condens. Matter Mater. Phys.* **2017**, *96*, 125429.
(40) Sobotík, P.; Kocán, P.; Ošťádal, I. Anisotropic alloying: Formation of atomic scale trellis on the Si(100)-(2 × 1) surface. *Surf. Sci.* **2018**, *677*, 8−11.
(41) Murata, Y.; Veronesi, S.; Whang, D.; Heun, S. Morphology of Ti on Monolayer Nanocrystalline Graphene and Its Unexpectedly Low Hydrogen Adsorption. *J. Phys. Chem. C* **2019**, *123*, 1572−1578.
(42) Büch, H.; Rossi, A.; Forti, S.; Convertino, D.; Tozzini, V.; Coletti, C. Superlubricity of epitaxial monolayer $WS_2$ on graphene. *Nano Res.* **2018**, *11*, 5946−5956.
(43) We note that structural optimization gives rise to a sliding of the layers in presence of interstitial Cu and a subsequent gap opening due to a partial decoupling of the layers. This behaviour is not expected to show up in real samples. We have thus chosen to mimic real samples by inhibiting layer sliding. In the latter case we find no significant gap opening.
(44) Babar, R.; Kabir, M. Transition Metal and Vacancy Defect Complexes in Phosphorene: A Spintronic Perspective. *J. Phys. Chem. C* **2016**, *120*, 14991−15000.
(45) Hu, T.; Hong, J. First-principles study of metal adatom adsorption on black phosphorene. *J. Phys. Chem. C* **2015**, *119*, 8199−8207.
(46) Liu, Q.; Zhang, X.; Abdalla, L. B.; Fazzio, A.; Zunger, A. Switching a Normal Insulator into a Topological Insulator via Electric Field with Application to Phosphorene. *Nano Lett.* **2015**, *15*, 1222−1228.
(47) Dolui, K.; Quek, S. Y. Quantum-confinement and Structural Anisotropy result in Electrically-Tunable Dirac Cone in Few-layer Black Phosphorous. *Sci. Rep.* **2015**, *5*, 11699.
(48) Zhang, C. D.; Lian, J. C.; Yi, W.; Jiang, Y. H.; Liu, L. W.; Hu, H.; Xiao, W. D.; Du, S. X.; Sun, L. L.; Gao, H. J. Surface Structures of


https://doi.org/10.1021/acs.jpcc.1c03531
J. Phys. Chem. C XXXX, XXX, XXX−XXX

Black Phosphorus Investigated with Scanning Tunneling Microscopy. *J. Phys. Chem. C* **2009**, *113*, 18823−18826.
(49) Schonenberger, C; Houten, H v.; Donkersloot, H C; Putten, A M T v. d.; Fokkink, L G J Single-electron tunneling up to room temperature. *Phys. Scr.* **1992**, *T45*, 289−291.
(50) Schonenberger, C; Houten, H. v.; Donkersloot, H. C Single-Electron Tunnelling Observed At Room Temperature by Scanning-Tunnelling Microscopy. *Europhysics Letters (EPL)* **1992**, *20*, 249−254.
(51) Dorogi, M.; Gomez, J.; Osifchin, R.; Andres, R. P.; Reifenberger, R. Room-temperature Coulomb blockade from a self-assembled molecular nanostructure. *Phys. Rev. B: Condens. Matter Mater. Phys.* **1995**, *52*, 9071−9077.
(52) Oncel, N.; Hallback, A.-S.; Zandvliet, H. J. W.; Speets, E. A.; Jan Ravoo, B.; Reinhoudt, D. N.; Poelsema, B. Coulomb blockade of small Pd clusters. *J. Chem. Phys.* **2005**, *123*, 044703.
(53) Hong, I-P.; Brun, C.; Pivetta, M.; Patthey, F.; Schneider, W.-D. Coulomb blockade phenomena observed in supported metallic nanoislands. *Front. Phys.* **2013**, *1*, 13.
(54) Brun, C.; Müller, K. H.; Hong, I.-P.; Patthey, F.; Flindt, C.; Schneider, W.-D. Dynamical Coulomb Blockade Observed in Nanosized Electrical Contacts. *Phys. Rev. Lett.* **2012**, *108*, 126802.
(55) Hanna, A. E.; Tinkham, M. Variation of the Coulomb staircase in a two-junction system by fractional electron charge. *Phys. Rev. B: Condens. Matter Mater. Phys.* **1991**, *44*, 5919−5922.
(56) Zhao, L.; He, R.; Rim, K. T.; Schiros, T.; Kim, K. S.; Zhou, H.; Gutiérrez, C.; Chockalingam, S. P.; Arguello, C. J.; Pálová, L.; et al. Visualizing Individual Nitrogen Dopants in Monolayer Graphene. *Science* **2011**, *333*, 999−1003.
(57) Betancur-Ocampo, Y.; Leyvraz, F.; Stegmann, T. Electron Optics in Phosphorene pn Junctions: Negative Reflection and Anti-Super-Klein Tunneling. *Nano Lett.* **2019**, *19*, 7760−7769.
(58) Giannozzi, P.; Baroni, S.; Bonini, N.; Calandra, M.; Car, R.; Cavazzoni, C.; Ceresoli, D.; Chiarotti, G. L.; Cococcioni, M.; Dabo, I.; et al. QUANTUM ESPRESSO: a modular and open-source software project for quantum simulations of materials. *J. Phys.: Condens. Matter* **2009**, *21*, 395502.
(59) Giannozzi, P; Andreussi, O; Brumme, T; Bunau, O; Buongiorno Nardelli, M; Calandra, M; Car, R; Cavazzoni, C; Ceresoli, D; Cococcioni, M; Colonna, N; Carnimeo, I; Dal Corso, A; de Gironcoli, S; Delugas, P; DiStasio, R A; Ferretti, A; Floris, A; Fratesi, G; Fugallo, G; Gebauer, R; Gerstmann, U; Giustino, F; Gorni, T; Jia, J; Kawamura, M; Ko, H-Y; Kokalj, A; Kucukbenli, E; Lazzeri, M; Marsili, M; Marzari, N; Mauri, F; Nguyen, N L; Nguyen, H-V; Otero-de-la-Roza, A; Paulatto, L; Ponce, S; Rocca, D; Sabatini, R; Santra, B; Schlipf, M; Seitsonen, A P; Smogunov, A; Timrov, I; Thonhauser, T; Umari, P; Vast, N; Wu, X; Baroni, S; et al. Advanced capabilities for materials modelling with Quantum ESPRESSO. *J. Phys.: Condens. Matter* **2017**, *29*, 465901.
(60) Perdew, J. P.; Burke, K.; Ernzerhof, M. Generalized Gradient Approximation Made Simple. *Phys. Rev. Lett.* **1996**, *77*, 3865−3868.
(61) Grimme, S. Semiempirical GGA-type density functional constructed with a long-range dispersion correction. *J. Comput. Chem.* **2006**, *27*, 1787−1799.
(62) Prandini, G.; Marrazzo, A.; Castelli, I. E.; Mounet, N.; Marzari, N. Precision and efficiency in solid-state pseudopotential calculations. *npj Comput. Mater.* **2018**, *4*, 72.
(63) Davey, W. P. Precision measurements of the lattice constants of twelve common metals. *Phys. Rev.* **1925**, *25*, 753−761.


https://doi.org/10.1021/acs.jpcc.1c03531
J. Phys. Chem. C XXXX, XXX, XXX−XXX